CASTING THE CORONAL MAGNETIC FIELD RECONSTRUCTION TOOLS IN 3D USING MHD BIFROST MODEL

Gregory Fleishman, Sergey Anfinogentov, Maria Loukitcheva, Ivan Mysh'yakov, and
Alexey Stupishin

01/01/2017

Research Team

Maria Loukitcheva
Expert user of Bifrost RMHD models; solar atmospheric models, solar chromosphere, chromospheric magnetography

Sergey Anfinogentov
Magnetic fields of the solar active regions; original π-disambiguation method and code; experienced user of 'Split' preprocessing

Alexey Stupishin
Magnetic fields of the active regions; developing algorithms and software for data processing and simulations; implementations of the weighted optimization method for NLFFF reconstruction and preprocessing

Ivan Mysh'yakov
Solar magnetic field of active regions; implementations of the full optimization method for NLFFF reconstruction

Introduction

- **A science question**: how accurate are the *static* tools that are currently used for a 3D reconstruction of the *dynamic* magnetic field from the photospheric vector boundary, namely (i) π-disambiguation tools; (ii) preprocessing tools; and (iii) 3D NLFFF reconstruction tools?
- **Methodology**: use the outcome of a full fledged *dynamic* RMHD model to perform "voxel-by-voxel" comparison of the restored magnetic field and the true magnetic field in the 3D model volume.

Plan of the Talk

- Description of the Bifrost code (Gudiksen et al. 2011) and the en024048_hion model used in our study (Carlsson et al. 2016); defining three reference layer used for the testing.
- π-disambiguation tools and their casting at the three layers.
- Preprocessing tools; assessment of their performance.
- Optimization methods for NLFFF reconstruction: weighted and full. Their performance for reconstructions starting from photospheric and chromospheric vector magnetograms. Critical assessment of the preprocessing impact and its need in the reconstruction techniques.
- Concluding remarks.

The en024048_hion model (Carlsson et al. 2016)

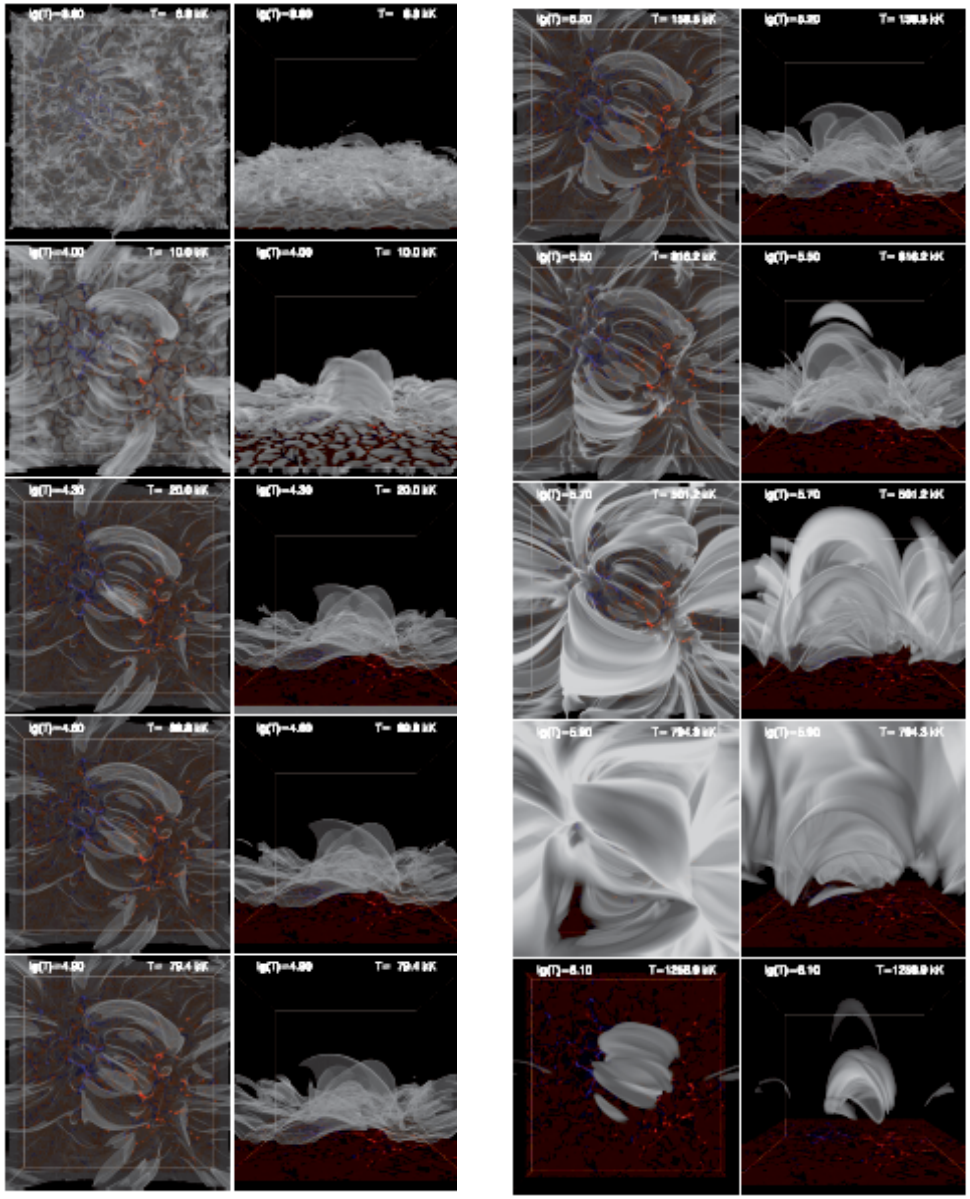

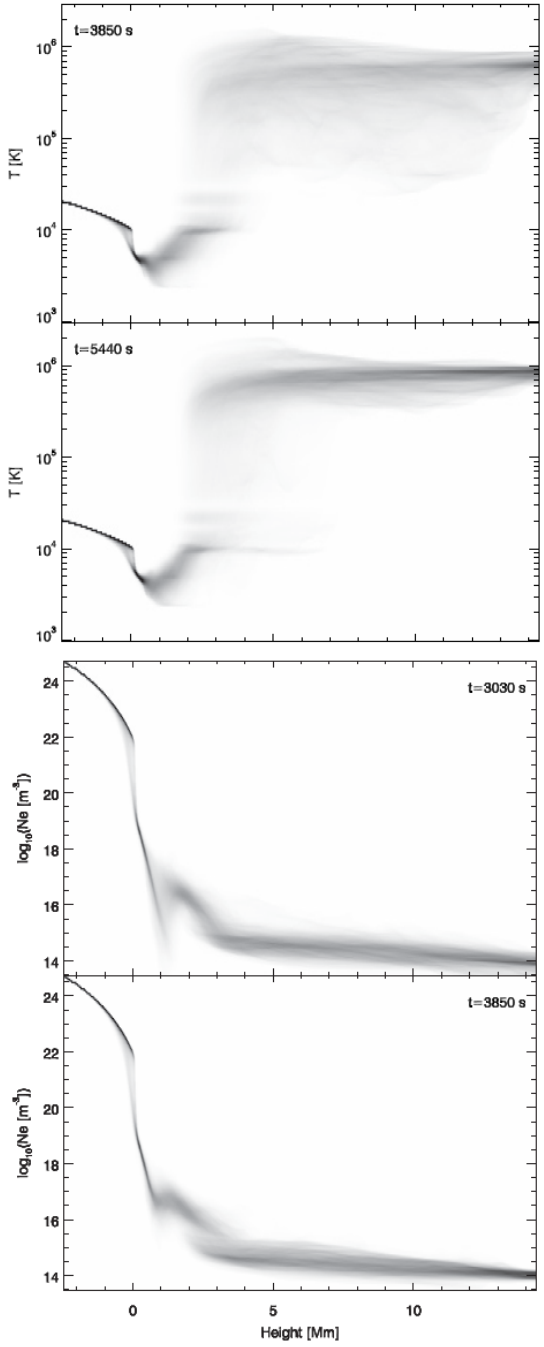

Electron temperature as a function of height

Snapshot t=3870 s
Z from 0 Mm to 5Mm

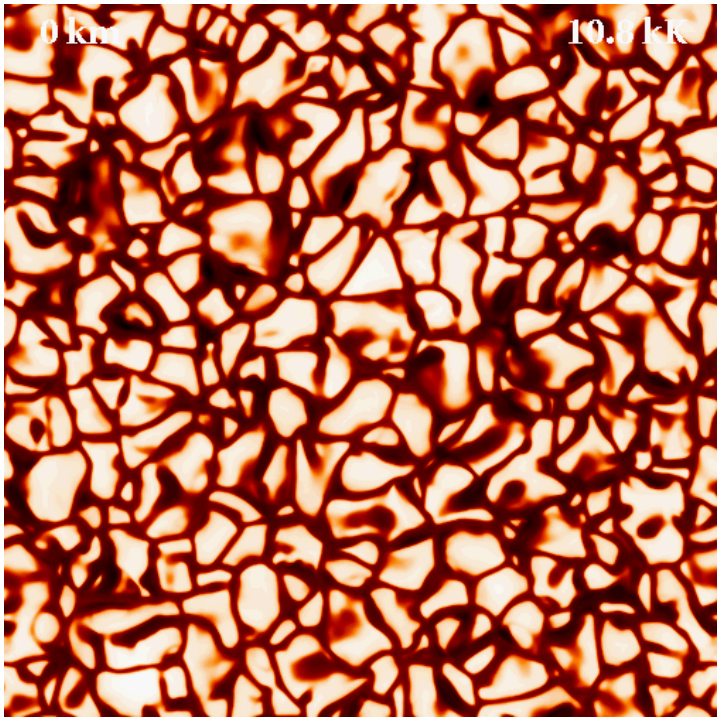

Distribution of magnetic field with height

Full cube:
Z from - 2.4Mm to 14.4Mm

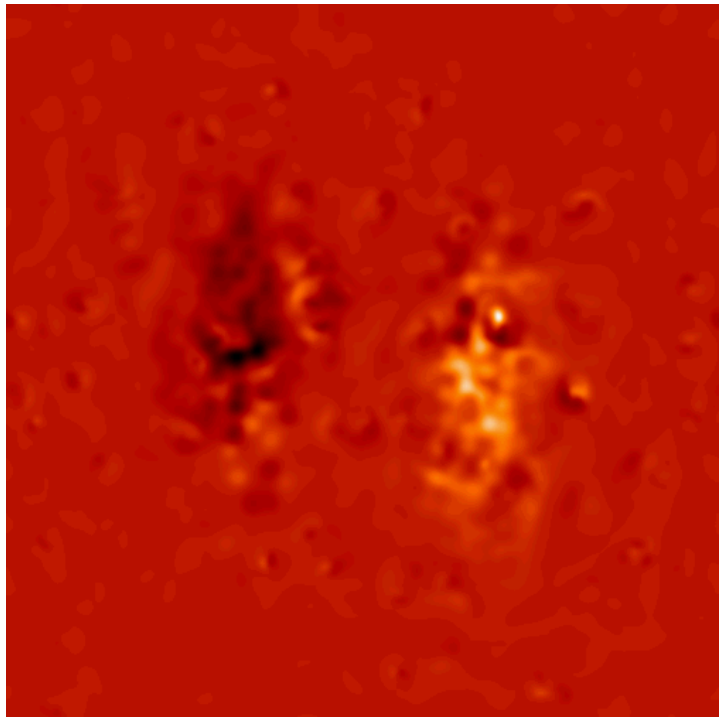

Force-freeness vs height

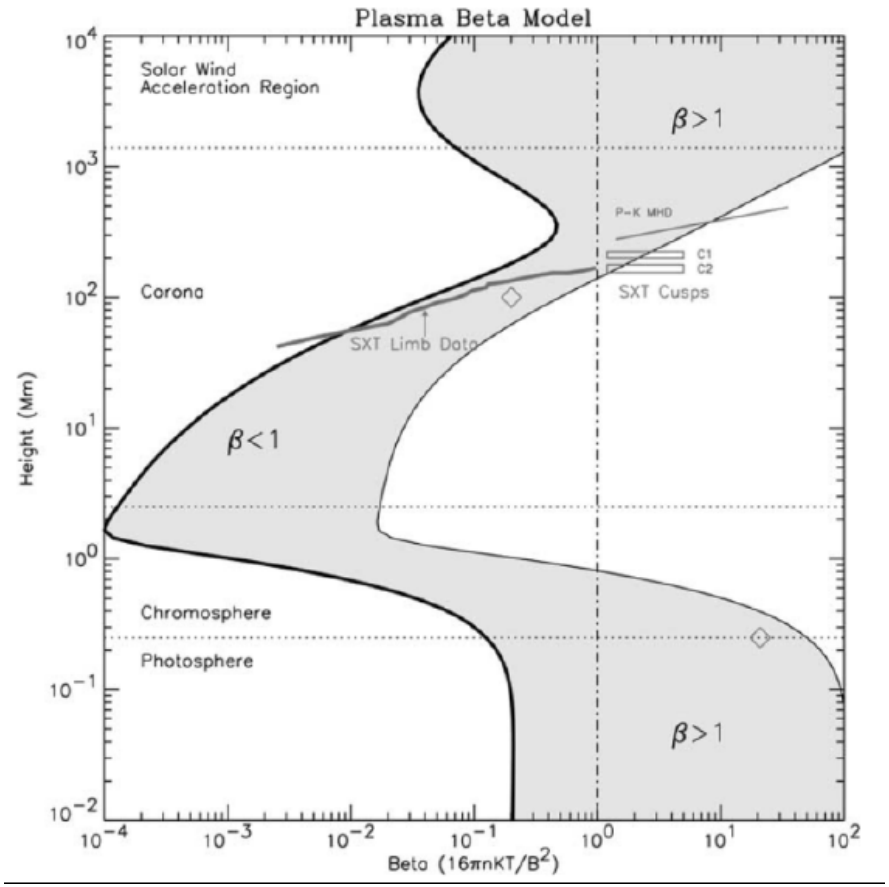

Gary 2001

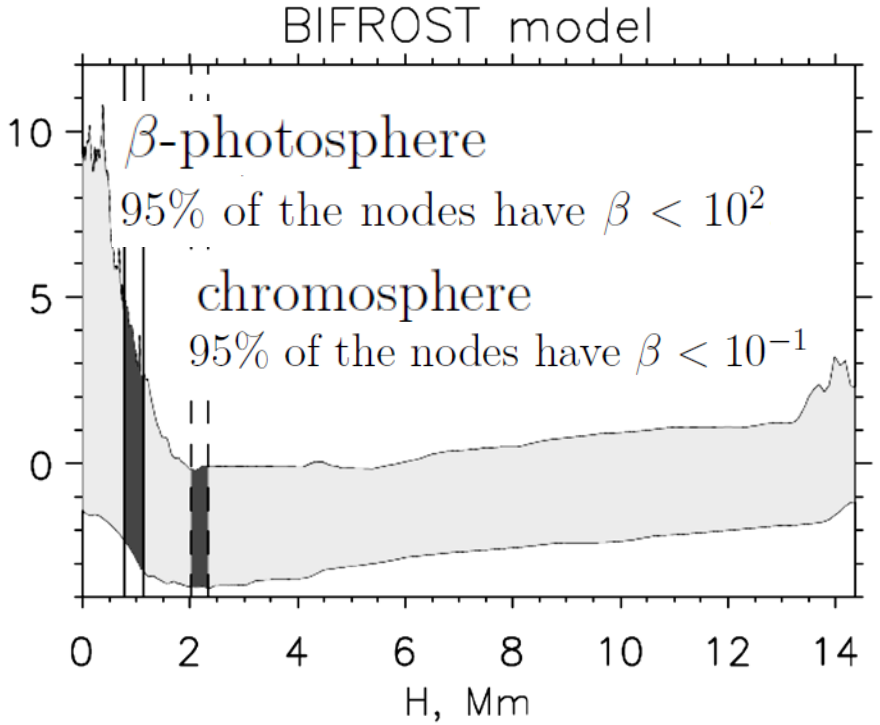

The magnetic topology is defined by two opposite polarity patches separated by 8 Mm with an average unsigned strength of 50 G in the photosphere, representing two patches of quiet-Sun network.

Bz vs height for various resolutions

Nominal photosphere

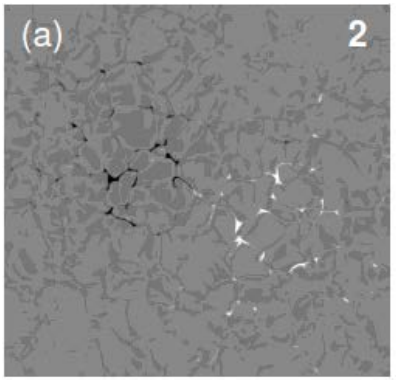

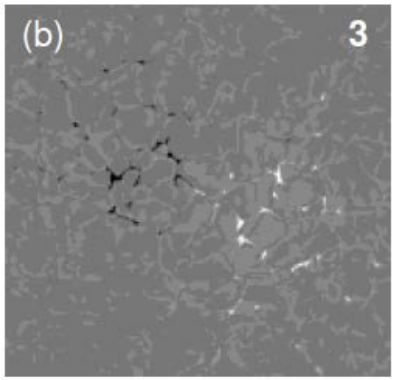

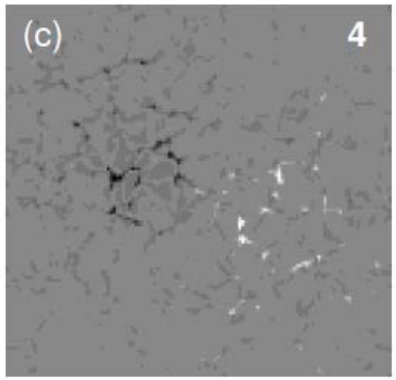

β-photosphere

$$\delta B_\alpha^2 = \frac{1}{n^3 - 1} \sum_{i=1}^{n^3} (B_\alpha[i] - \overline{B}_\alpha)^2$$

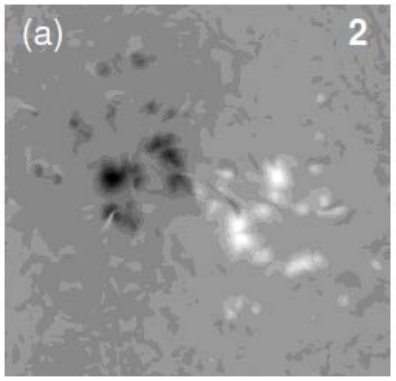

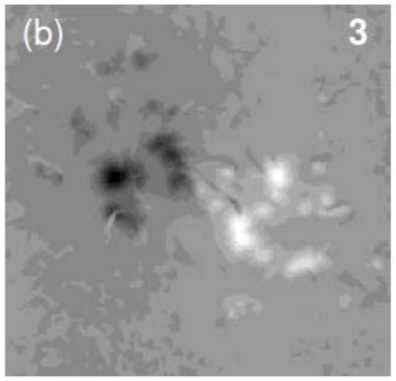

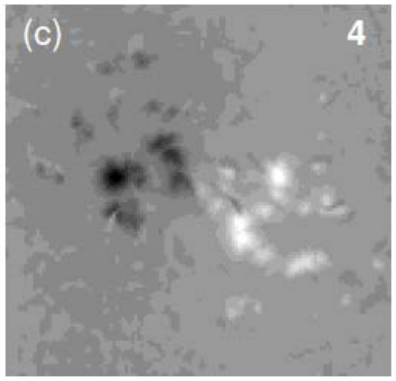

Chromosphere

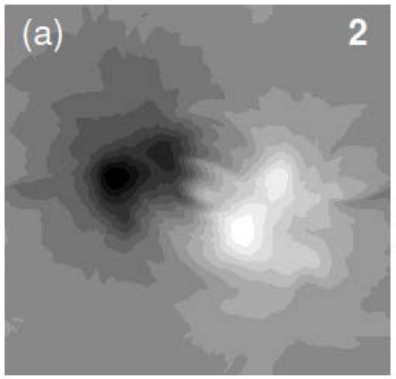

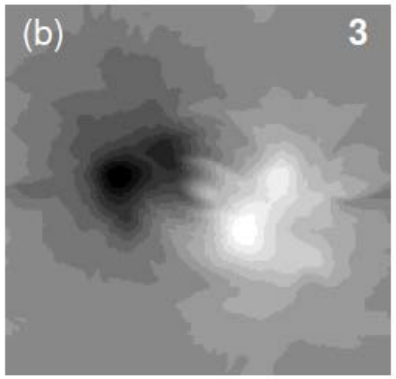

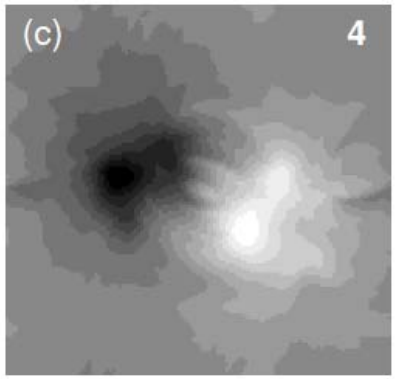

$n = 2,\ 3,\ 4,\ 6,\ 7,\ 9$

Various resolutions and force-free metrics

$\alpha = x,\ y,\ \text{or}\ z.$ $n = 2,\ 3,\ 4,\ 6,\ 7,\ 9$

$$\overline{B}_\alpha = \frac{1}{n^3}\sum_{i=1}^{n^3} B_\alpha[i] \qquad \delta B_\alpha^2 = \frac{1}{n^3-1}\sum_{i=1}^{n^3}(B_\alpha[i] - \overline{B}_\alpha)^2$$

$$\theta = arcsin\left(\frac{\sum_i^N \sigma_i}{N}\right), \quad \theta_j = arcsin\left(\frac{\sum_i^N |\boldsymbol{j}|_i\,\sigma_i}{\sum_i^N |\boldsymbol{j}|_i}\right)$$

$$\sigma_i = \frac{|\boldsymbol{j}\times\boldsymbol{B}|_i}{|\boldsymbol{j}|_i\,|\boldsymbol{B}|_i},$$

Sine of mismatch angle between vectors

$$f = \frac{1}{N}\sum_i^N \frac{|\nabla \boldsymbol{B}|_i}{6\,|\boldsymbol{B}|_i} dx$$

Measure of the field divergence

Force-free metrics depending on resolutions

Binning factor	Volume above	layer #	θ°	θ_j°	$f \times 10^6$
1	Nominal photosphere	0	19.23	48.60	568
	β-photosphere	17	17.21	18.65	158
	chromosphere	42	16.23	5.59	107
2	Nominal photosphere	0	18.59	46.00	1573
	β-photosphere	8	16.65	18.57	401
	chromosphere	21	15.55	5.97	245
3	Nominal photosphere	0	18.48	43.93	2594
	β-photosphere	6	16.32	14.70	609
	chromosphere	14	15.37	6.41	410

π-DISAMBIGUATION TESTS

$$E_{\text{pix}} = \frac{N_{\text{err}}}{N},$$

$$E_{\text{flux}} = \frac{\sum_{\text{err}} B_\tau(x,y)}{\sum_{\text{all}} B_\tau(x,y)},$$

Nominal photosphere

	Pixel error, %			Flux error, %			Computation time	
Bin	SFQ	ME	AA	SFQ	ME	AA	SFQ	ME
2	19.5	20.5	30.3	18.8	14.8	28.4	2.9s	13m57s
3	19.0	23.9	30.3	19.2	16.4	27.7	1.4s	6m30s
4	19.2	27.6	29.6	20.4	18.7	26.6	0.7s	4m04s
6	14.3	34.2	28.0	14.0	27.0	25.3	0.38s	1m46s
7	12.3	33.0	26.8	12.8	26.2	23.9	0.31s	1m18s
9	8.6	33.0	23.5	9.1	27.8	19.0	0.18s	48s

Chromosphere

β-photosphere

	Pixel error, %			Flux error, %			Pixel error, %			Flux error, %			Computation time	
Bin	SFQ	ME	AA	SFQ	ME	AA	SFQ	ME	AA	SFQ	ME	AA	SFQ	ME
2	0.005	0	5.0	0.0001	0	1.5	1.7	5.8	8.1	0.6	2.3	3.5	1.1s	8m38s
3	0.007	0	4.9	0.0003	0	1.4	1.3	3.1	6.3	0.4	1.0	2.5	0.37s	3m39s
4	0.03	0.013	4.6	0.006	0.0004	1.3	1.3	2.3	6.7	0.4	0.71	2.7	0.18s	2m11s
6	0.06	0.014	4.7	0.014	0.0005	1.4	0.76	0.4	5.7	0.15	0.045	2.1	0.09s	3m56s
7	0.06	0	4.6	0.02	0	1.3	0.46	0.21	5.8	0.11	0.016	2.0	0.09s	3m39s
9	0.03	0	4.4	0.01	0	1.3	0.63	0.35	5.6	0.21	0.027	2.0	0.02s	26s

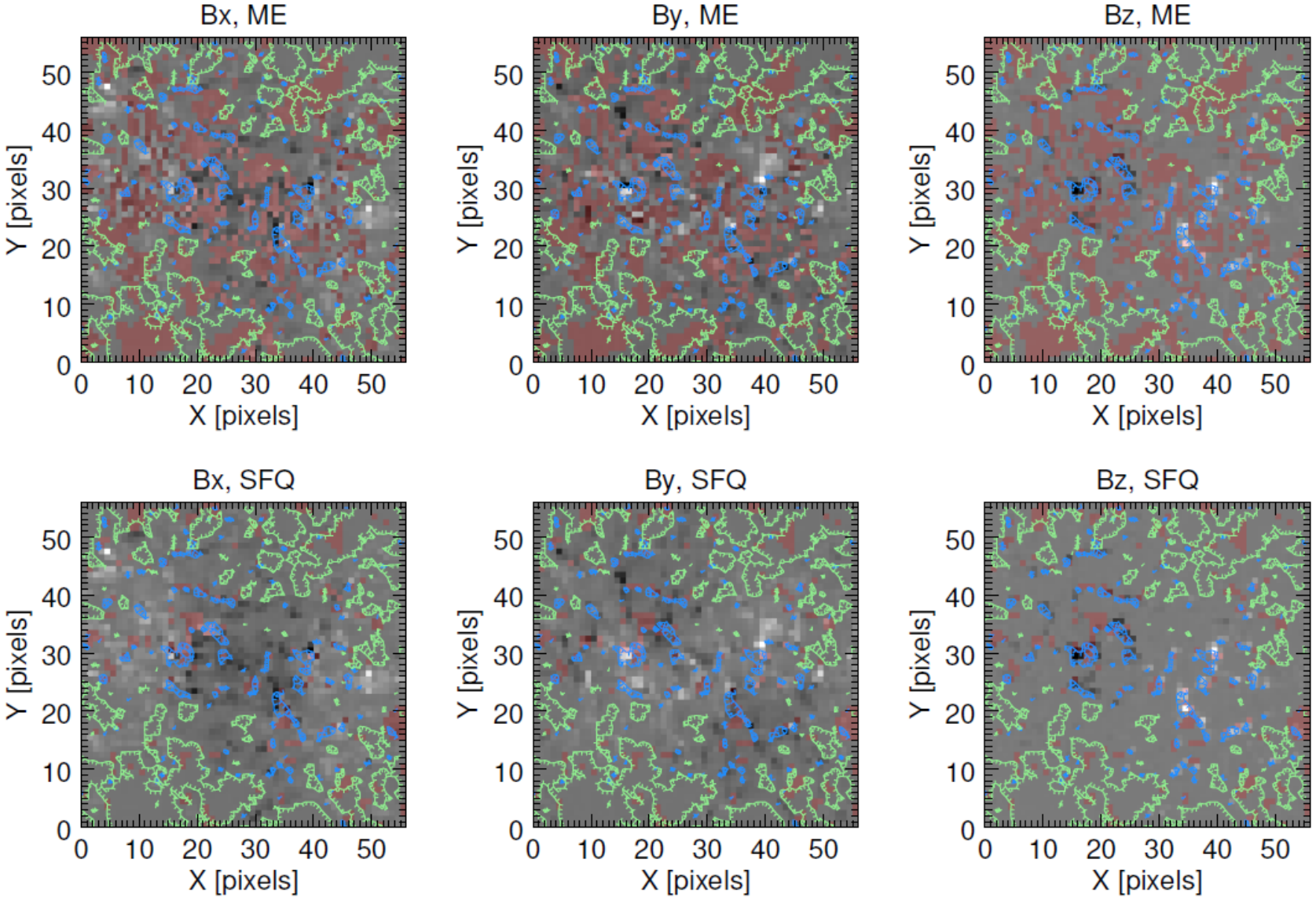

Comparison of the disambiguation results of the ME (top row) and SFQ (bottom row) codes for the BIFROST field with the binning factor 9 at the level of **nominal photosphere**. Pixels with the disambiguation errors are indicated in the semitransparent red. Blue contours enclose regions with almost vertical magnetic field (inclination angle < 15 degrees). Green contours enclose weak field regions where B < 50 G. Ticks on the contours show the direction towards the lower values.

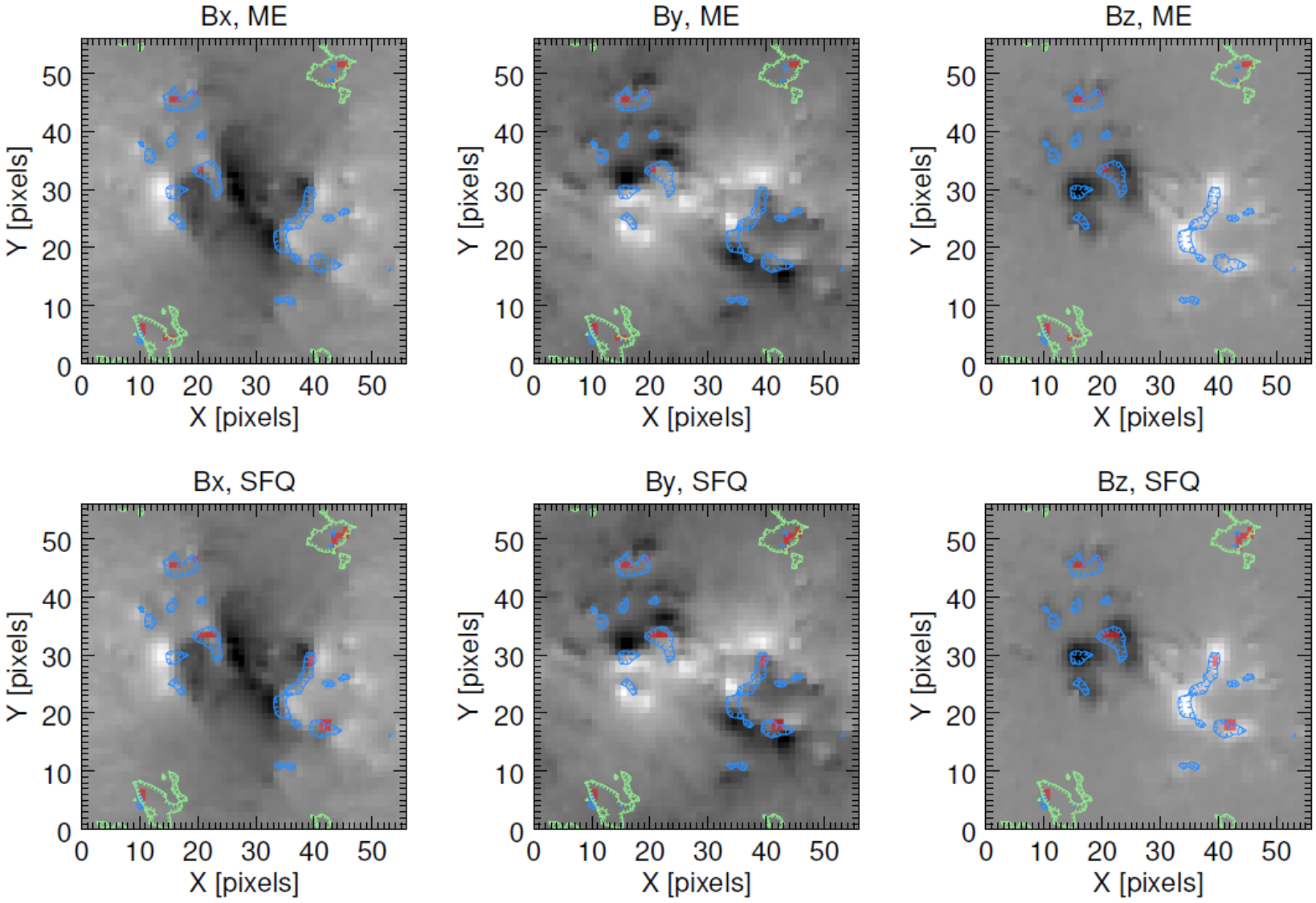

Comparison of the disambiguation results of the ME (top row) and SFQ (bottom row) codes for the BIFROST field with the binning factor 9 at the level of **correct β photosphere**. Pixels with the disambiguation errors are indicated in the semitransparent red. Blue contours enclose regions with almost vertical magnetic field (inclination angle < 15 degrees). Green contours enclose weak field regions where B < 50 G. Ticks on the contours show the direction towards the lower values.

Preprocessing

$$\tilde{L_3} = \sqrt{\frac{L_3}{\sum_p B^2}}, \qquad E_B = \sqrt{\frac{\sum_p (\tilde{B} - B)^2}{\sum_p B^2}},$$

$$\tilde{B} = SB + b$$

$$S = \frac{\sum_p \tilde{B}B - \sum_p \tilde{B} \sum_p B/N}{\sum_p B^2 - (\sum_p B)^2/N}$$

Expected: $S = 1$; b=0

In practice $S \neq 1$

in most cases

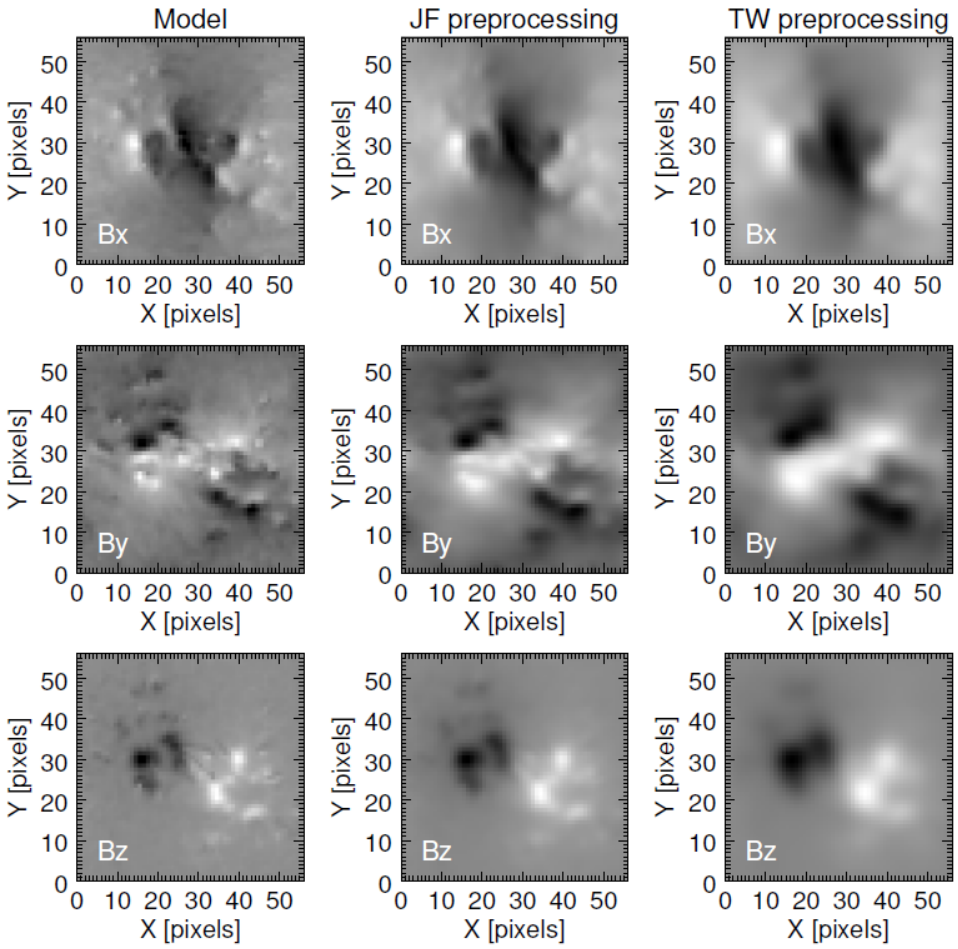

Jiang, C., & Feng, X. 2014, SoPh, 289, 63 Wiegelmann, T., Inhester, B., & Sakurai, T. 2006

Preprocessing – tests

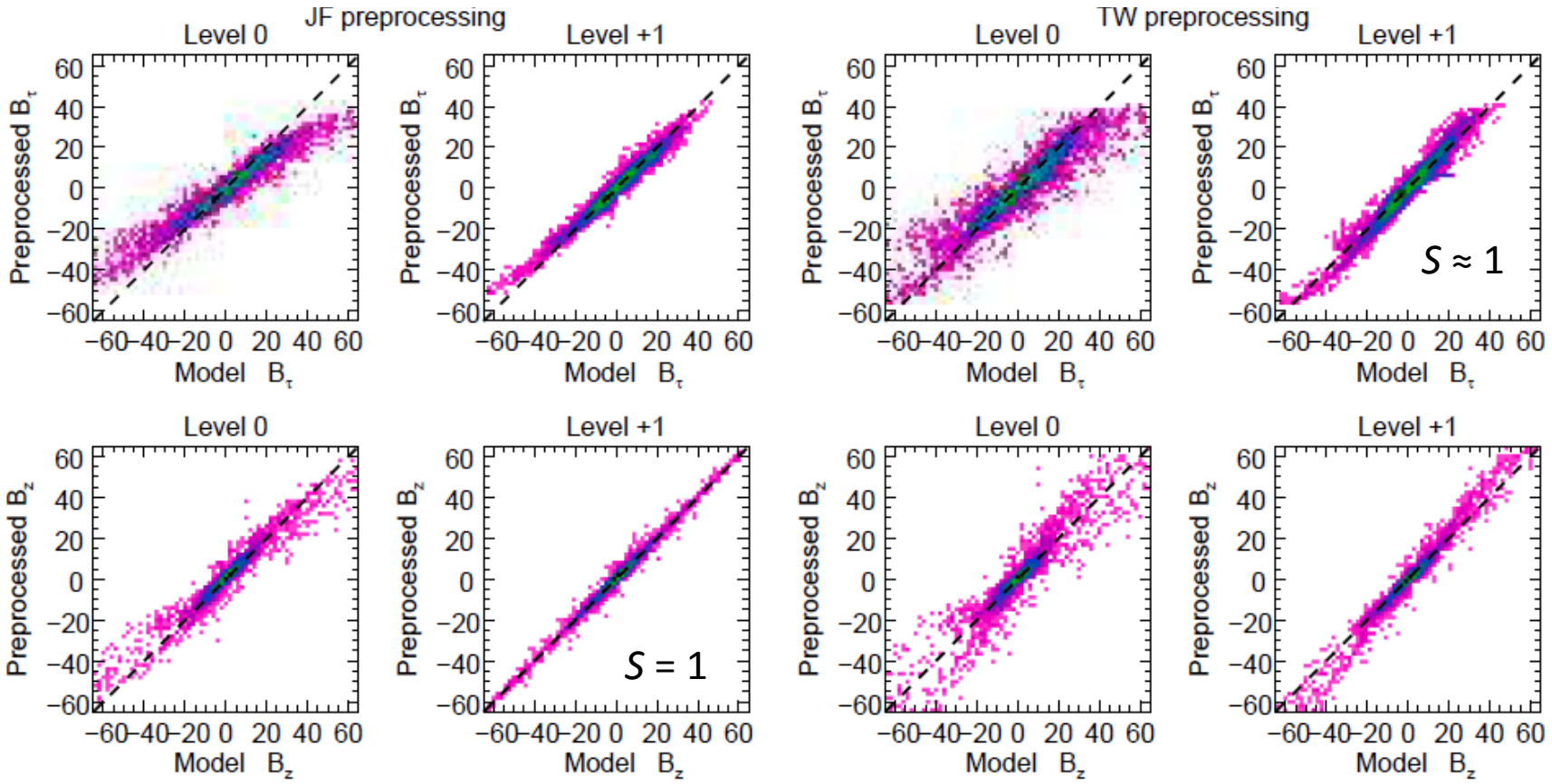

Extrapolations – tests

$S = 1$

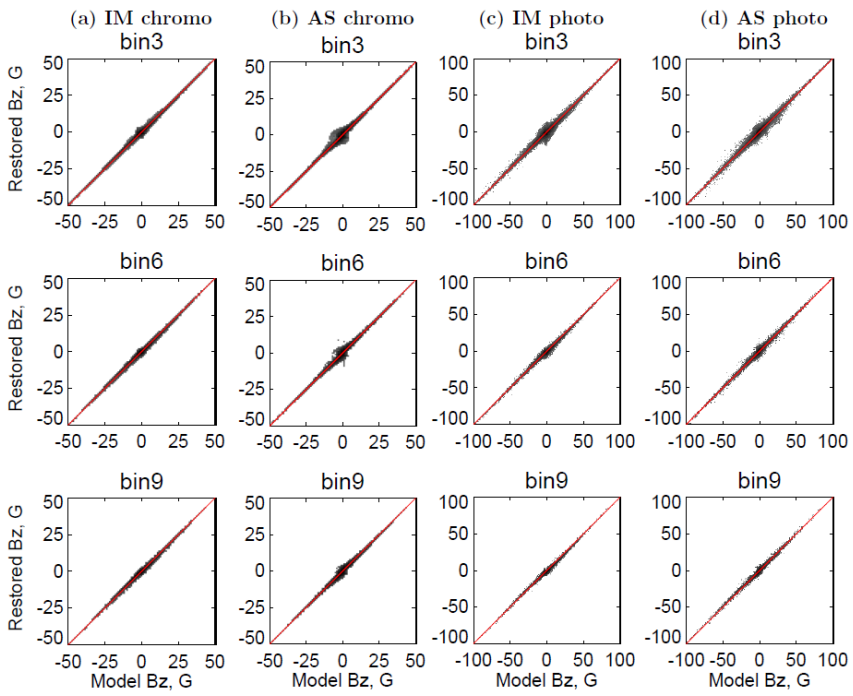

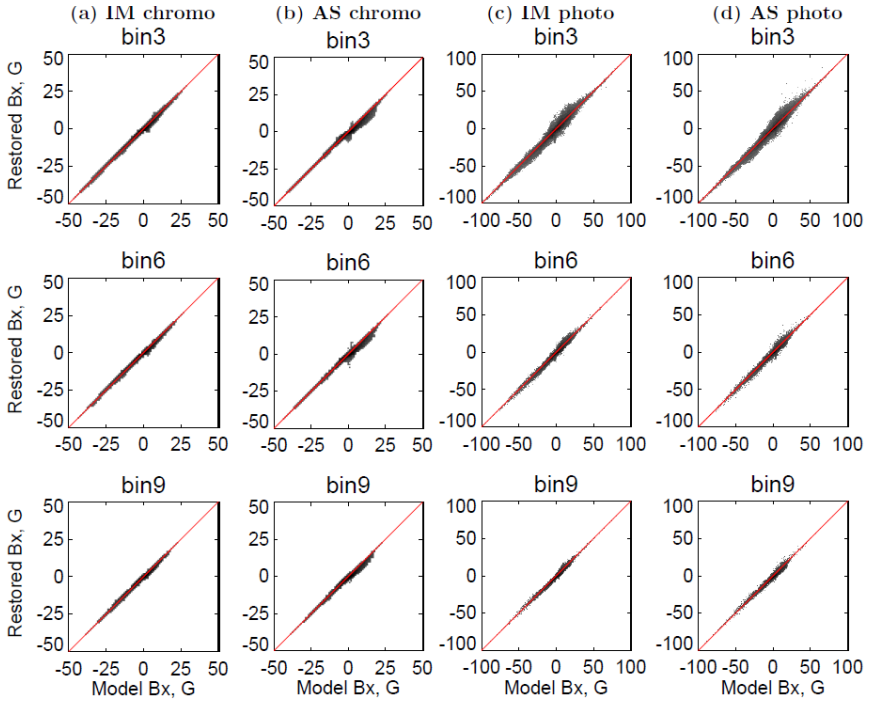

Extrapolation error at a few levels: B_z starting from chromospheric level

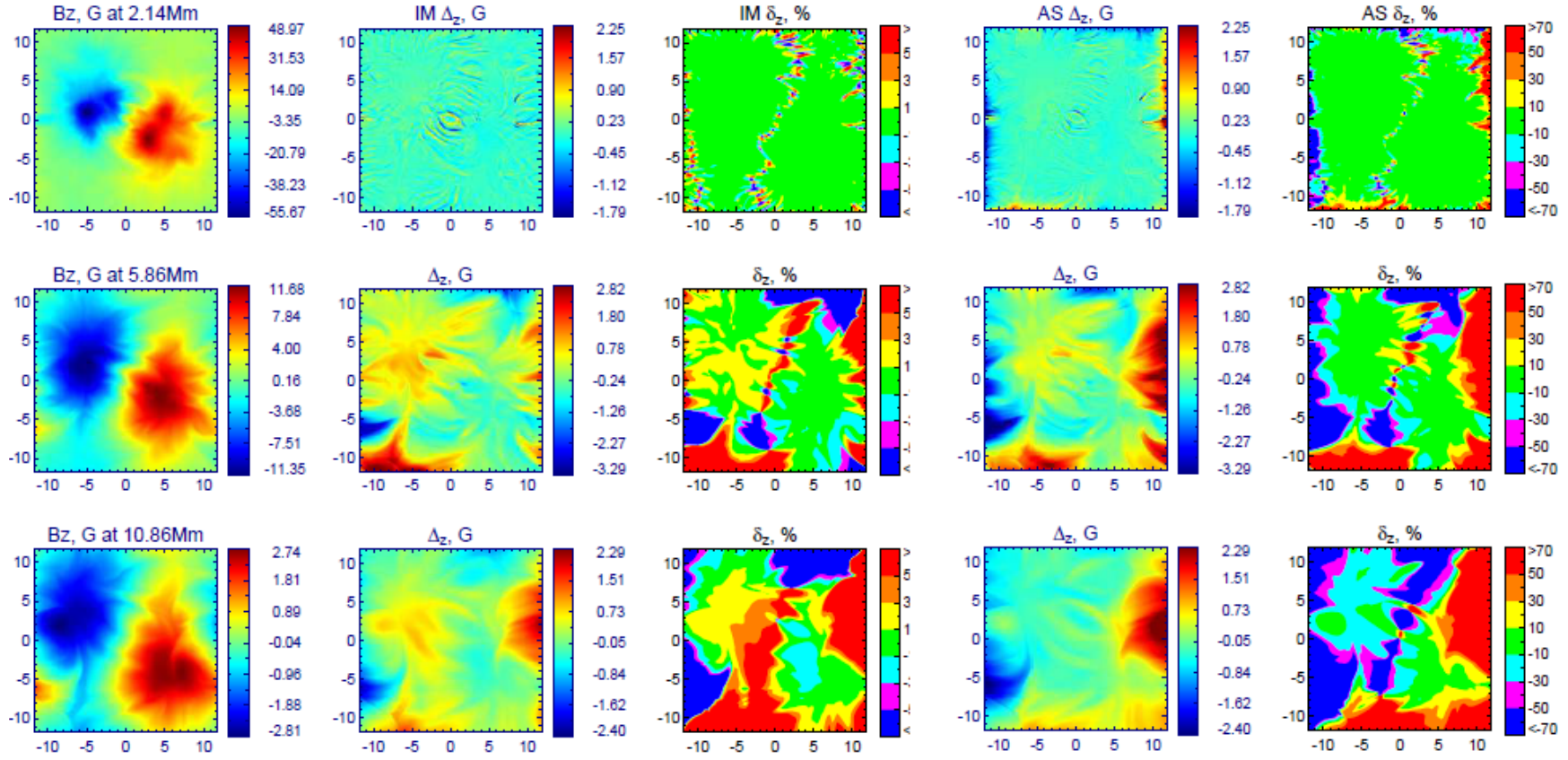

$$\Delta_\alpha[j] = B_{\mathrm{NLFFF},\alpha}[j] - \overline{B}_\alpha[j], \qquad \delta_\alpha[j] = \frac{B_{\mathrm{NLFFF},\alpha}[j] - \overline{B}_\alpha[j]}{\langle \overline{B}_\alpha[j] \rangle}, \qquad \alpha = x,\ y,\ \text{or } z,$$

Extrapolation error at a few levels: B_y starting from chromospheric level

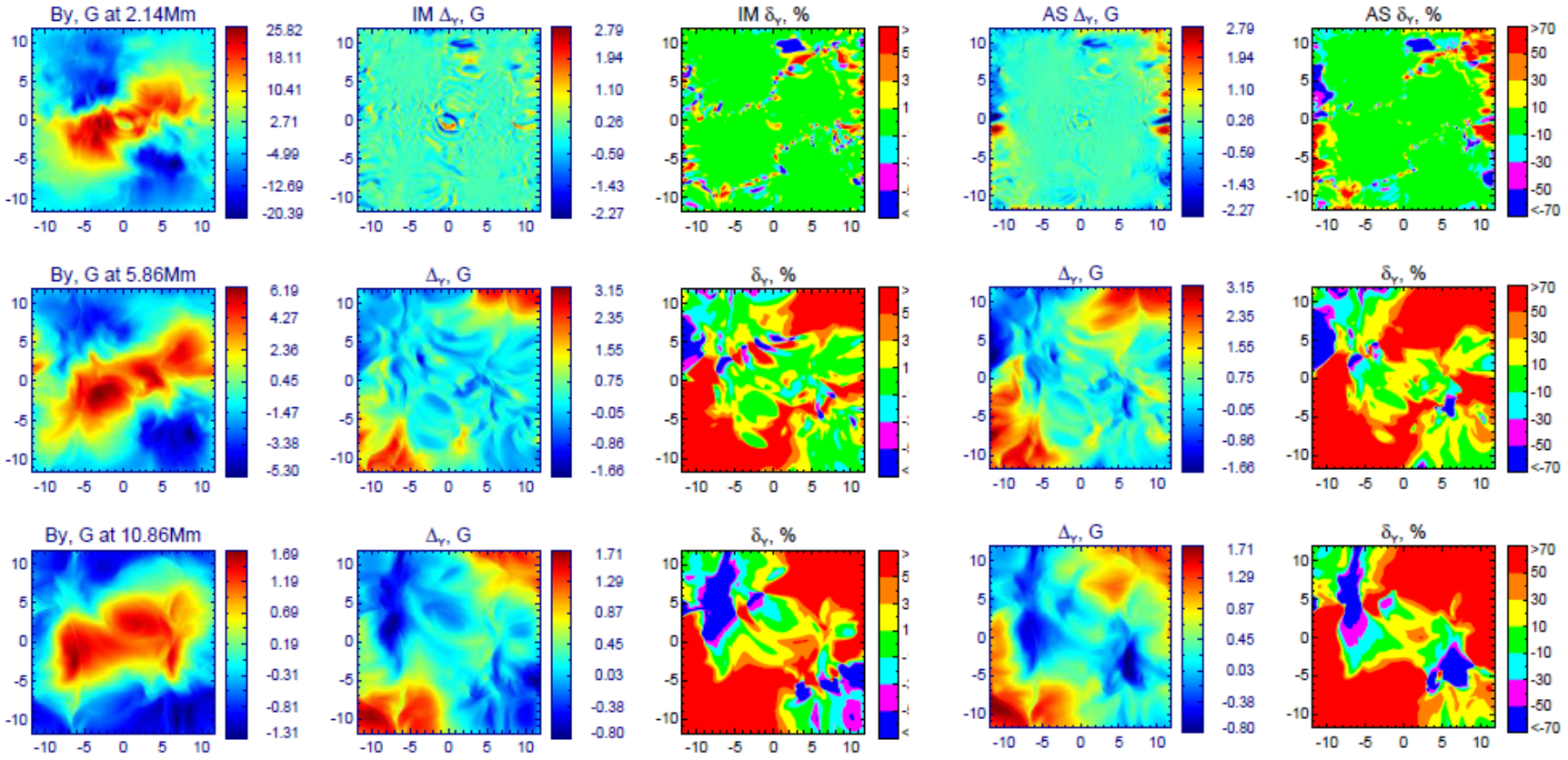

Extrapolation error at a few levels: B_z starting from photospheric level

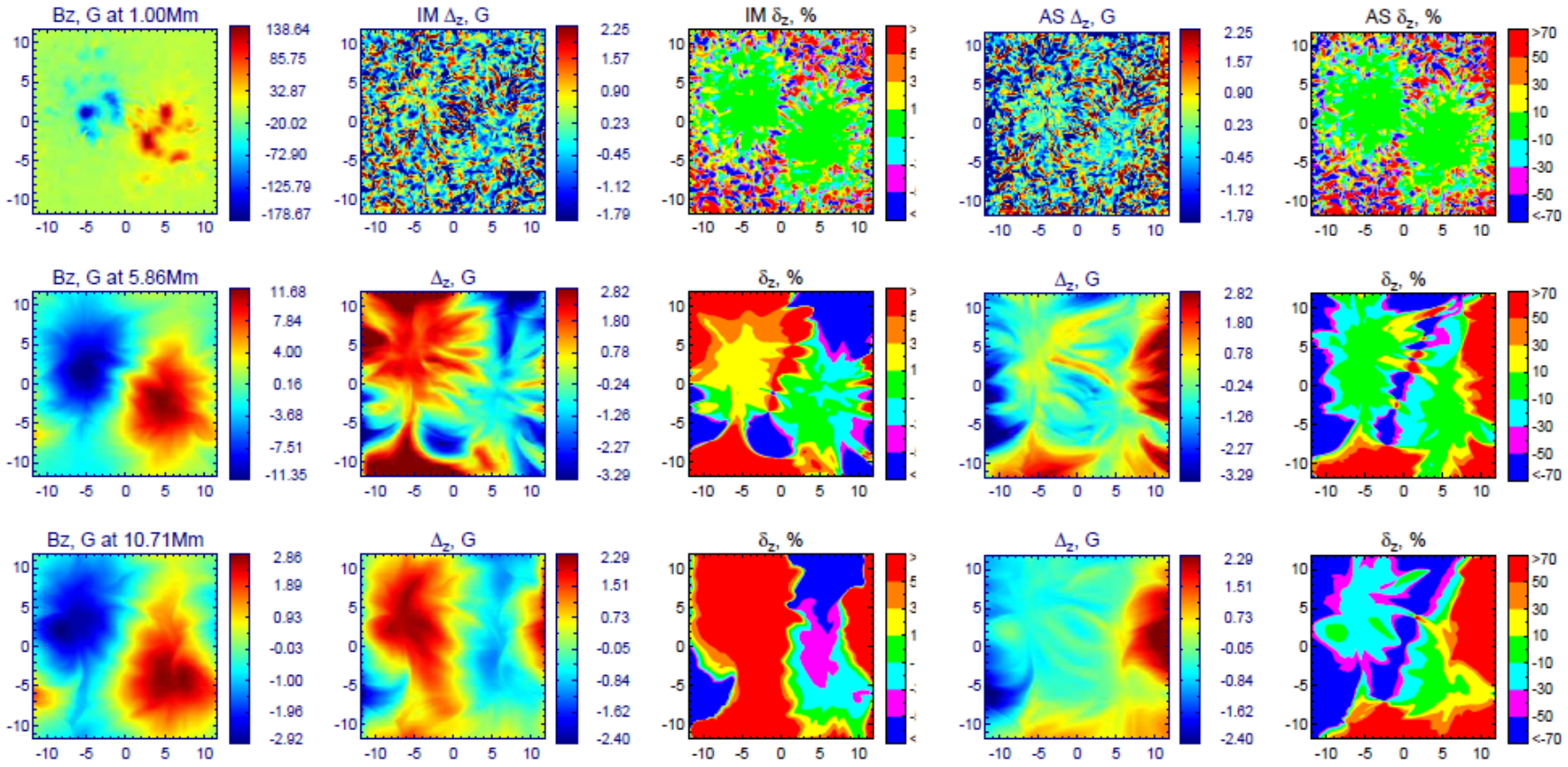

Normalized residuals vs height; no preprocessing

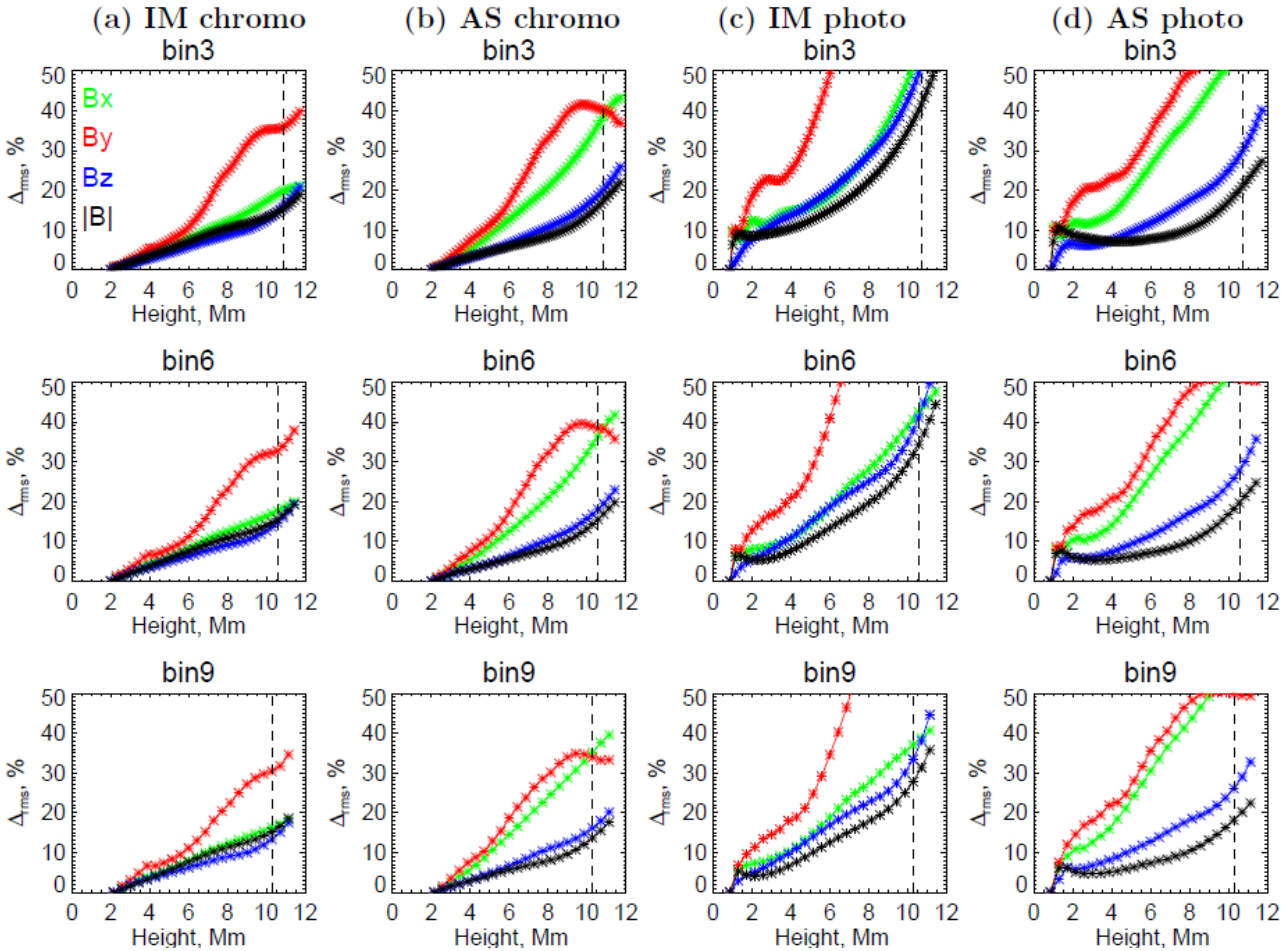

$$\Delta_{\mathrm{rms},\alpha} = = \sqrt{\frac{\sum_{j=1}^{N_{\mathrm{vox}}} \Delta_\alpha^2[j]}{\sum_{j=1}^{N_{\mathrm{vox}}} \overline{B}_\alpha^2[j]}},$$

$$\alpha = x,\ y,\ \text{or}\ z$$

Table 13. Normalized rms error after preprocessing at a given level for bin-factor 9.

	$\Delta_{rms}(B)$				$\Delta_{rms}(Bx)$				$\Delta_{rms}(By)$				$\Delta_{rms}(Bz)$			
	JF		TW		JF		TW		JF		TW		JF		TW	
Level, Mm	IM	AS	IM	AS	IM	AS	IM	AS	IM	AS	IM	AS	IM	AS	IM	AS
1.29	11.74	11.74	18.52	18.52	49.39	49.39	59.91	59.91	53.99	53.99	62.80	62.80	43.53	43.53	56.00	56.00
1.71	10.20	10.62	15.88	16.19	57.55	60.68	63.15	67.46	58.04	75.16	67.31	81.91	42.61	40.57	49.65	47.24
2.14	9.26	11.65	14.66	17.41	57.71	63.22	66.38	72.56	63.11	112.86	71.07	128.83	40.51	42.27	47.20	53.71
2.57	8.86	12.26	13.99	18.46	55.86	62.28	68.84	71.48	66.53	157.49	76.49	174.11	37.28	42.30	43.73	52.01
3.00	8.69	12.49	13.30	18.31	59.76	64.16	73.87	67.36	86.77	219.79	99.08	244.61	36.86	43.26	45.01	45.72
3.43	8.79	12.83	12.71	18.49	63.75	67.47	79.79	71.74	115.00	264.09	123.13	295.16	42.79	58.30	54.18	57.00
3.86	9.24	12.91	12.32	18.34	68.76	76.11	87.46	74.34	119.52	209.52	125.65	238.25	44.34	58.69	57.04	56.78
4.29	9.81	13.12	11.95	18.28	77.17	86.33	101.38	84.83	119.39	166.58	125.54	192.68	48.39	78.24	59.27	78.25
4.71	10.40	13.17	11.42	18.37	92.92	98.20	125.24	95.05	120.45	166.99	128.14	193.75	51.69	75.26	57.69	71.12
5.14	11.06	13.13	10.92	18.17	86.43	105.57	119.66	101.92	136.51	201.81	147.75	237.17	58.54	82.58	58.61	84.14
5.57	11.84	13.23	10.69	18.36	82.65	117.65	116.60	112.03	173.13	229.95	178.85	268.30	70.34	86.36	64.69	89.18
6.00	12.71	13.46	10.75	18.53	76.01	120.13	109.49	115.10	206.64	241.49	205.23	285.48	76.77	88.02	69.53	92.58
6.43	13.74	13.87	11.15	19.07	78.13	133.96	106.72	129.77	243.42	268.11	245.12	312.53	77.84	89.20	71.81	95.07
6.86	14.67	14.01	11.54	19.34	84.33	146.48	104.80	141.80	210.74	223.94	204.64	263.12	78.33	97.22	74.96	103.99
7.29	15.73	14.64	12.25	20.48	87.35	158.28	100.91	154.88	225.33	229.43	217.68	266.84	79.19	105.43	74.85	113.87
7.71	16.96	15.73	13.23	21.98	92.34	169.14	108.47	166.54	254.39	243.45	251.71	284.09	86.63	122.39	77.93	132.37
8.14	18.36	16.89	14.46	23.76	95.86	179.78	111.08	179.02	274.37	257.53	280.08	299.48	101.12	144.44	84.03	157.78
8.57	19.88	18.29	15.87	25.53	100.29	190.13	113.97	189.64	287.52	262.93	300.73	305.69	115.77	162.48	90.98	177.24
9.00	21.59	19.83	17.45	27.68	106.53	200.27	121.84	200.94	306.10	283.20	335.13	327.94	116.86	160.11	89.20	175.69
9.43	23.76	21.92	19.41	30.11	112.49	206.55	129.09	208.11	328.16	318.05	374.39	367.12	123.33	163.78	90.70	179.46
9.86	26.38	24.33	21.73	33.08	119.47	211.15	135.16	215.00	325.05	331.21	380.54	379.92	143.46	180.35	104.73	198.94
10.29	29.27	26.70	24.18	35.67	127.75	215.23	143.72	220.97	303.74	306.72	356.55	350.54	168.32	198.96	123.37	219.53
10.71	32.69	29.16	27.12	38.61	136.22	224.39	164.62	233.03	321.87	317.83	380.88	361.37	204.36	219.73	157.59	243.95
11.14	36.57	31.54	30.78	41.03	150.26	233.82	196.81	246.27	330.97	336.39	402.63	380.18	248.93	243.80	202.33	270.82

Extrapolations from a preprocessed boundary

Expected: $\tilde{B} = SB + b$

with S = 1; b=0

In practice S ≠ 1

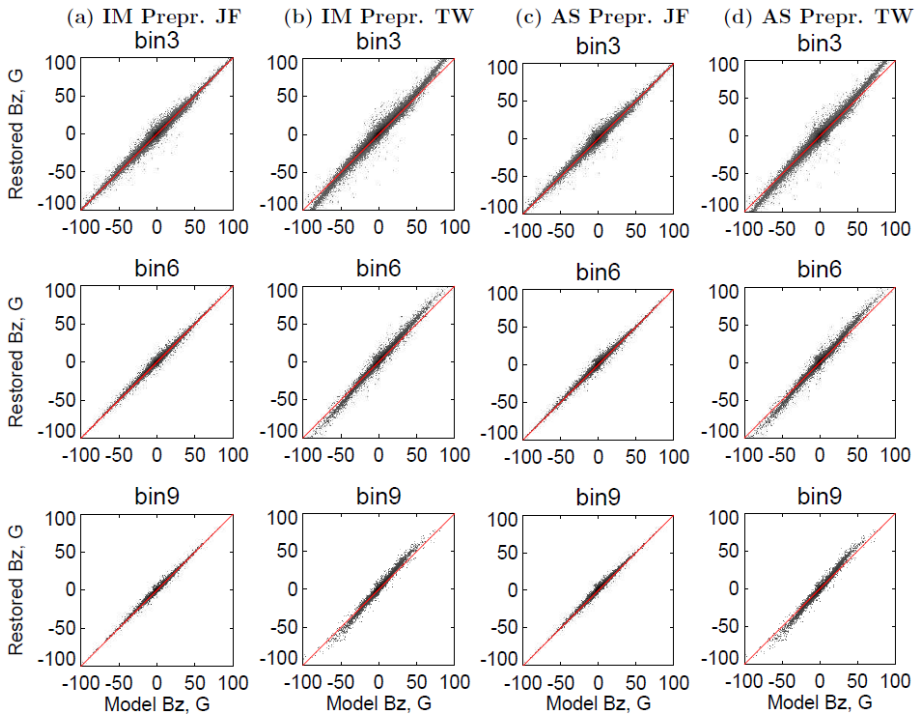

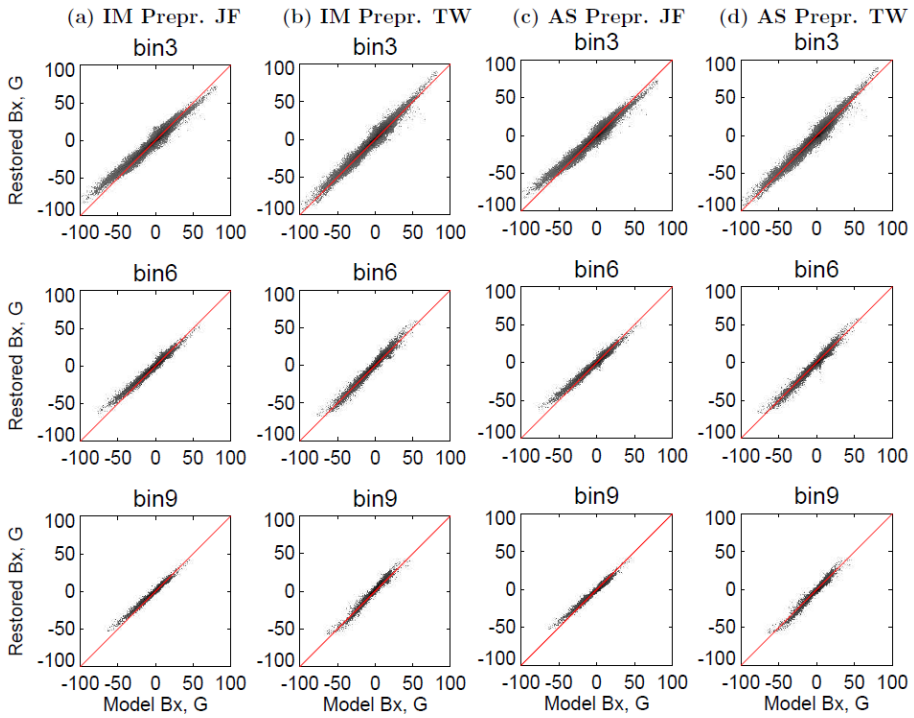

Normalized residuals vs height; with preprocessing

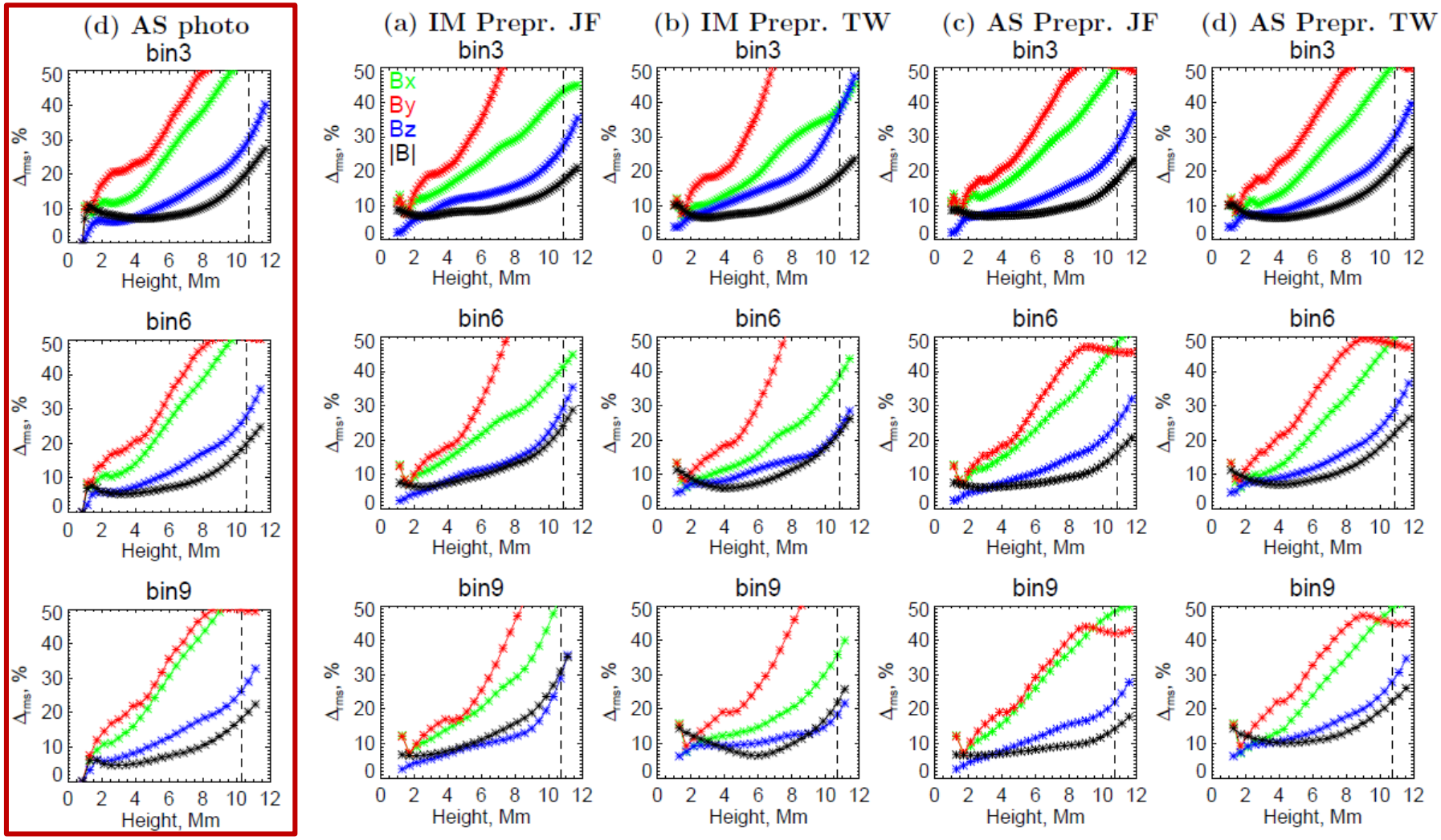

No preprocessing for comparison

Table 14. Normalized rms residual after preprocessing at a given level for bin-factor 9.

	$\Delta_{rms}(B)$				$\Delta_{rms}(Bx)$				$\Delta_{rms}(By)$				$\Delta_{rms}(Bz)$			
	JF		TW		JF		TW		JF		TW		JF		TW	
Level, Mm	IM	AS	IM	AS	IM	AS	IM	AS	IM	AS	IM	AS	IM	AS	IM	AS
1.29	6.71	6.71	14.38	14.38	12.35	12.35	15.86	15.86	12.07	12.07	15.43	15.43	2.56	2.56	6.31	6.31
1.71	6.47	6.56	13.10	12.64	7.15	7.19	7.54	7.14	7.26	7.18	9.18	9.21	3.60	3.60	7.62	7.46
2.14	6.43	6.56	12.14	12.07	8.98	9.20	9.28	8.84	9.91	10.47	11.50	12.54	4.42	4.69	9.16	9.21
2.57	6.60	6.57	11.31	11.37	10.28	10.90	10.50	10.51	12.41	13.58	13.51	15.35	4.96	5.43	9.48	9.73
3.00	6.84	6.64	10.49	11.01	11.31	12.06	11.11	11.00	14.28	15.62	15.28	17.54	5.47	6.05	9.41	9.90
3.43	7.21	6.79	9.66	10.46	12.57	13.48	11.79	11.98	15.76	17.38	17.16	19.58	6.11	6.84	9.37	10.16
3.86	7.68	6.93	8.85	10.26	13.88	15.30	12.21	13.11	17.01	19.08	19.12	22.04	6.70	7.47	9.32	10.44
4.29	8.19	7.13	8.10	10.05	15.08	16.87	12.43	14.19	16.70	19.07	19.00	22.31	7.39	8.39	9.36	10.91
4.71	8.84	7.34	7.42	10.14	16.25	19.25	12.91	16.70	17.31	20.47	19.44	23.89	8.16	9.13	9.51	11.41
5.14	9.55	7.66	6.88	10.21	17.54	21.30	13.47	18.79	19.23	22.77	21.31	26.23	8.81	10.04	9.69	12.05
5.57	10.26	7.89	6.55	10.54	18.80	23.77	14.02	21.51	22.13	26.27	23.83	29.70	9.29	10.72	9.86	12.59
6.00	11.08	8.23	6.50	10.74	20.37	26.06	14.80	23.87	25.41	29.23	26.63	32.71	9.72	11.59	10.14	13.30
6.43	12.03	8.52	6.78	11.10	22.34	28.70	15.84	26.58	28.94	31.92	29.53	35.56	10.15	12.40	10.56	14.08
6.86	13.02	8.84	7.37	11.41	24.49	31.06	17.11	28.90	32.90	33.65	32.79	37.61	10.58	13.39	11.09	15.05
7.29	14.04	9.06	8.21	12.03	26.38	33.33	18.36	31.35	37.65	36.44	37.07	40.37	11.04	14.25	11.65	16.07
7.71	15.11	9.32	9.20	12.65	27.95	35.11	19.52	33.33	42.28	38.81	41.49	42.62	11.64	15.13	12.23	17.11
8.14	16.19	9.49	10.26	13.61	29.49	37.07	20.78	35.69	47.00	41.23	45.97	44.62	12.30	15.72	12.62	18.10
8.57	17.39	9.76	11.41	14.55	31.64	39.14	22.49	38.08	51.25	43.25	50.21	46.46	13.06	16.18	12.73	18.96
9.00	18.92	10.13	12.76	15.89	34.66	41.35	24.62	40.58	53.99	43.98	53.18	47.18	14.37	16.65	12.94	20.05
9.43	20.97	10.78	14.43	17.12	38.38	43.51	27.02	43.03	55.70	43.69	55.03	46.94	16.51	17.47	13.53	21.37
9.86	23.62	11.68	16.47	18.82	42.74	45.43	29.65	45.29	57.09	42.94	56.39	46.11	19.58	18.58	14.57	23.21
10.29	26.86	12.83	18.91	20.27	47.67	46.98	32.54	47.25	58.92	42.37	58.11	45.57	23.65	20.05	16.15	25.15
10.71	30.75	14.26	21.92	22.29	53.28	48.30	35.83	49.05	61.39	41.95	60.32	45.00	28.95	22.00	18.44	27.88
11.14	35.14	15.86	25.78	23.83	59.84	49.27	39.93	50.64	65.55	42.02	64.00	44.76	35.67	24.46	21.70	30.62

Conclusions

- Here we have demonstrated that a realistic MHD model, in the presented case – a 'en024048_hion' simulation (Carlsson et al. 2016) obtained with the Bifrost code (Gudiksen et al. 2011), can be very efficiently utilized to cast various tools used for the coronal magnetic field reconstruction. In particular, we have evaluated the performance of the π-disambiguation codes, magnetogram preprocessing codes, and NLFFF extrapolation codes developed following the optimization method (Wheatland et al. 2000).
- We have found that the currently used **π-disambiguation** codes work pretty well at the AR photosphere and chromosphere, but often fail at the quiet sun photosphere. This can become important when a question of the magnetic field at the quiet sun is specifically addressed. Here we are primarily interested in the performance of the reconstruction tools in ARs; thus, we adopted that the π-ambiguity has been perfectly resolved.
- Then, we have assessed the performance of two different **preprocessing** approaches aimed to improve the bottom boundary condition toward force-freeness. Although the tested preprocessing codes do produce a more force-free boundary, there is an unsolicited byproduct of these preprocessings – the poorly controlled elevation of the magnetic field components, which are different for the longitudinal and transverse field components. This mismatch results in a poorly controlled systematic error in the height scale in the extrapolated data cube.
- On the other hand, comparison between the volumetric metrics of the magnetic data cubes extrapolated from the photospheric level either with or without preprocessing are not much different from each other, while extrapolation without preprocessing preserves the correct height scale. From this perspective, **we conclude that the use of NLFFF extrapolation from the actual photospheric magnetogram (without any preprocessing** but instead, perhaps, with some sort of smoothing suppressing the noise in the original data) **is preferable**.